NeuroImage: Clinical 16 (2017) 564–574

Contents lists available at ScienceDirect

NeuroImage: Clinical

journal homepage: www.elsevier.com/locate/ynicl

Advancing functional dysconnectivity and atrophy in progressive supranuclear palsy

Jesse A. Brown[a], Alice Y. Hua[a], Andrew Trujillo[a], Suneth Attygalle[a], Richard J. Binney[b], Salvatore Spina[a], Suzee E. Lee[a], Joel H. Kramer[a], Bruce L. Miller[a], Howard J. Rosen[a], Adam L. Boxer[a], William W. Seeley[a,c,*]

[a] Memory and Aging Center, Department of Neurology, University of California San Francisco, San Francisco, CA, USA
[b] Temple University, Eleanor M. Saffran Center for Cognitive Neuroscience, Department of Communication Sciences and Disorders, Philadelphia, PA, USA
[c] Department of Pathology, University of California, San Francisco, USA

ARTICLE INFO

Keywords:
Progressive supranuclear palsy
Longitudinal
Intrinsic connectivity network
Modularity

ABSTRACT

Progressive supranuclear palsy syndrome (PSP-S) results from neurodegeneration within a network of brainstem, subcortical, frontal and parietal cortical brain regions. It is unclear how network dysfunction progresses and relates to longitudinal atrophy and clinical decline. In this study, we evaluated patients with PSP-S (n = 12) and healthy control subjects (n = 20) at baseline and 6 months later. Subjects underwent structural MRI and task-free functional MRI (tf-fMRI) scans and clinical evaluations at both time points. At baseline, voxel based morphometry (VBM) revealed that patients with mild-to-moderate clinical symptoms showed structural atrophy in subcortex and brainstem, prefrontal cortex (PFC; supplementary motor area, paracingulate, dorsal and ventral medial PFC), and parietal cortex (precuneus). Tf-fMRI functional connectivity (FC) was examined in a rostral midbrain tegmentum (rMT)-anchored intrinsic connectivity network that is compromised in PSP-S. In healthy controls, this network contained a medial parietal module, a prefrontal-paralimbic module, and a subcortical-brainstem module. Baseline FC deficits in PSP-S were most severe in rMT network integrative hubs in the prefrontal-paralimbic and subcortical-brainstem modules. Longitudinally, patients with PSP-S had declining intermodular FC between the subcortical-brainstem and parietal modules, while progressive atrophy was observed in subcortical-brainstem regions (midbrain, pallidum) and posterior frontal (perirolandic) cortex. This suggested that later-stage subcortical-posterior cortical change may follow an earlier-stage subcortical-anterior cortical disease process. Clinically, patients with more severe baseline impairment showed greater subsequent prefrontal-parietal cortical FC declines and posterior frontal atrophy rates, while patients with more rapid longitudinal clinical decline showed coupled prefrontal-paralimbic FC decline. VBM and FC can augment disease monitoring in PSP-S by tracking the disease through stages while detecting changes that accompany heterogeneous clinical progression.

1. Introduction

Patients with progressive supranuclear palsy syndrome (PSP-S) exhibit gait disturbance with early falls, axial rigidity, and supranuclear gaze palsy (Steele et al., 1964), accompanied by executive dysfunction and bradyphrenia (Bak et al., 2005; Bruns and Josephs, 2013; Burrell et al., 2014; Dubois et al., 1988; Pillon et al., 1995). Structural MRI reveals prominent atrophy involving the dorsal midbrain and superior cerebellar peduncle, often extending to the thalamus, basal ganglia, frontal operculum, dorsal insula, supplementary motor areas, and the dorsolateral prefrontal cortex (Boxer et al., 2006; Ghosh et al., 2012; Shang et al., 2014; Whitwell et al., 2011). Intrinsic functional connectivity (FC) reductions appear in a network anchored by the rostral midbrain tegmentum (rMT), an area of peak atrophy in PSP-S (Boxer et al., 2006; Gardner et al., 2013; Whitwell et al., 2011). Many rMT network regions, which include the pons, cerebellum, midbrain, thalamus, basal ganglia, insula, frontal, and parietal cortex, show FC deficits in the absence of atrophy, suggesting that tissue dysfunction may precede measurable neuronal and synaptic volume loss (Gardner et al., 2013).

At autopsy, most patients with PSP syndrome show progressive supranuclear palsy (PSP) histopathology, a four-repeat tauopathy (Litvan et al., 1996; Steele et al., 1964). Patients with more advanced clinical PSP-S show more widespread tau aggregation (Williams et al.,

* Corresponding author at: UCSF Memory and Aging Center, Department of Neurology, 675 Nelson Rising Lane, San Francisco, CA 94158, USA.
E-mail address: bill.seeley@ucsf.edu (W.W. Seeley).

http://dx.doi.org/10.1016/j.nicl.2017.09.008
Received 11 April 2017; Received in revised form 1 August 2017; Accepted 6 September 2017
Available online 12 September 2017

2007). Williams and colleagues proposed a staging system for PSP in which tau aggregates are confined to the subthalamic nucleus, pallidum, and substantia nigra at stage 1, the posterior frontal cortex and cerebellar dentate nucleus at stage 2, and the parietal lobe at stage 3. While staging patients based on postmortem tau aggregation gives the impression of progressive disease spread, it cannot by its nature determine whether individuals follow this sequence during life. If the disease advances through consistent stages, patients with intermediate levels of clinical impairment – those most likely to be enrolled in a study and capable of receiving structural and functional MRI scans – might be expected to show greatest baseline atrophy and functional dysconnectivity in "stage 1" regions and the greatest subsequent longitudinal decline in "stage 2" and "stage 3" regions.

Clinical deficits in PSP-S can be assessed using the PSP rating scale (PSPRS), which measures symptom severity for daily activities, behavior, and function in the bulbar, oculomotor, limb motor, and gait/midline domains (Golbe and Ohman-Strickland, 2007). Patients progress an average of 10 points per year (Golbe, 2014), and a worsening PSPRS correlates with progressive atrophy in the frontal lobe and midbrain (Josephs et al., 2013). Progressive atrophy further involves the midbrain, pons, superior cerebellar peduncle, frontal/parietal/temporal cortex, thalamus, caudate, and pallidum (Josephs et al., 2013) (Paviour et al., 2006) (Dutt et al., 2016). Based on structural MRI measures, such as the rate of midbrain atrophy over 12 months, power analyses have estimated that 77 subjects would be required to detect a 25% treatment effect with 90% power, versus 152 subjects for PSPRS (Dutt et al., 2016). In the current study, we aimed to assess and compare task-free fMRI (tf-fMRI) and structural MRI as biomarkers of PSP-S progression in patients with mild to moderate clinical disease severity.

When considering disease progression biomarkers, it is critical to establish goals for the biomarker, including how it relates to clinical progression and how it would be used in a clinical trial. In this study, we evaluated four biomarker-to-clinical relationship categories: 1) biomarker change that predicts subsequent clinical change, 2) biomarker change synchronized with clinical change, 3) biomarker change that is dependent on the level of baseline clinical severity, and 4) biomarker change that occurs independent of clinical progression. We examined the relative rates of tf-fMRI, structural MRI, and PSPRS change over 6 months in patients with PSP-S and healthy controls to assess the potential of functional and structural neuroimaging as biomarkers for PSP-S. This study addressed one primary hypothesis and one open question. We hypothesized that longitudinal FC declines and atrophy would roughly follow a stage-wise progression from subcortical to frontal and eventually to parietal areas. We assessed the open question of whether FC baseline deficits in PSP-S vulnerable brain regions would precede subsequent clinical decline.

2. Material and methods

2.1. Subjects

Subjects were evaluated at the University of California, San Francisco (UCSF) Memory and Aging Center. All subjects or their surrogates provided informed consent according to the Declaration of Helsinki and the procedures were approach by the Institutional Review Board at UCSF. Twelve patients with PSP-S were included, having met the following inclusion criteria: (1) a research diagnosis of possible or probable PSP syndrome, based on the Litvan criteria (Litvan et al., 1996). 7 subjects had a diagnosis of PSP-Probable and 5 had a diagnosis of PSP-Possible. In all patients with a PSP-Possible diagnosis, there was either vertical gaze palsy or slowing of vertical saccades and postural instability with falls in the first year since disease onset, along with axial rigidity, indicative of PSP-Richardson's syndrome, and in none of the 12 patients was there responsiveness to levodopa, asymmetric parkinsonian signs, or tremor that would be indicative of PSP Parkinsonism (Williams et al., 2005); (2) no significant history of other neurological diseases or structural brain abnormalities inconsistent with PSP, (3) baseline and follow-up fMRI scans with acceptable levels of head motion (see Methods) within 180 ± 30 days of one another. We ensured that all tf-fMRI scans had head motion < 3 mm of maximum relative translation, 3° of maximum relative rotation, and fewer than than 10% of frames with 1 mm motion "spikes". A subset of 4 patients had autopsy data and all showed a primary pathological diagnosis of PSP. Six subjects were taking dopaminergic medications, four of whom were also receiving anti-depressants (SSRI or tricyclic). Subject medications remained unchanged during the study interval. Patients underwent a full baseline clinical evaluation including a history, a general neurological examination, Mini-Mental State Exam (MMSE) testing, and Clinical Dementia Rating (CDR). Subjects were rated on the PSPRS at both time points (Golbe and Ohman-Strickland, 2007) and received a battery of bedside neuropsychological tests at baseline (Table 1) (Rosen et al., 2002).

Table 1
Subject characteristics. CDR: Clinical Dementia Rating; PSPRS: PSP Rating Scale; MMSE: Mini-Mental State Exam; BNT: Boston Naming Test.

	PSP-S Mean ± SD	n	Healthy controls Mean ± SD	n	HC–PSP-S p-value
Age at baseline, years	69.0 ± 7.4	12	66.2 ± 7.0	20	0.28
Sex (F:M)	6:6	12	12:8	20	–
Education, years	16.6 ± 3.5	12	16.7 ± 2.0	20	0.86
Interscan interval, days	183 ± 14	12	192 ± 17	20	0.11
CDR total, baseline	0.5 ± 0.4	11	0 ± 0	**9**	< 0.001
CDR total, follow up	0.3 ± 0.3	9	0 ± 0	**3**	–
CDR, sum of boxes, baseline	3.0 ± 2.7	11	0 ± 0	**9**	< 0.001
CDR, sum of boxes, follow up	2.1 ± 1.9	9	0 ± 0	**3**	–
PSPRS baseline	27.6 ± 10.6	12	0	14	< 0.001
PSPRS follow up	33.9 ± 13.2	12	0	7	–
MMSE, baseline (max 30)	26.2 ± 3.8	11	29.5 ± 0.8	20	< 0.001
BNT (max 15)	13.5 ± 1.7	10	14.8 ± 0.4	20	< 0.001
Digit span (backward)	3.6 ± 1.2	9	5.5 ± 1.5	20	< 0.001
Modified trails (correct lines/min)	16.7 ± 8.6	11	47.2 ± 24.1	20	< 0.001
Letter fluency	6.9 ± 4.6	11	16.4 ± 4.7	16	< 0.001
Semantic fluency	13.8 ± 6.9	9	23.4 ± 5.7	20	< 0.001
fMRI Head max translation, mm, baseline	0.81 ± 0.33	12	0.70 ± 0.35	20	0.35
fMRI Head max translation, mm, follow up	0.98 ± 0.56	12	0.59 ± 0.38	20	0.03
fMRI Head max rotation, °, baseline	0.55 ± 0.34	12	0.51 ± 0.27	20	0.76
fMRI Head max rotation, °, follow up	0.68 ± 0.55	12	0.39 ± 0.15	20	0.03
fMRI Head sum displacement, mm, baseline	36.5 ± 16.0	12	41.0 ± 23.0	20	0.55
fMRI Head sum displacement, mm, follow up	47.0 ± 27.3	12	37.0 ± 23.7	20	0.28

Twenty age- and sex-matched healthy control (HC) subjects were included in the study and met the same criteria as the patients for interscan interval and tf-fMRI motion levels. The 20 controls had a CDR score of 0 at both time points, a MMSE score of 27 or higher, and no significant history of neurological disease or gross structural brain abnormalities. All subjects received the same battery of bedside neuropsychological tests.

The University of California San Francisco Committee on Human Research approved the study. Participants provided informed consent prior to participation.

2.2. Neuroimaging

All subjects were scanned at the UCSF Neuroscience Imaging Center on a Siemens Trio 3T scanner. A T1-weighted MP-RAGE structural scan was acquired with an acquisition time = 8 min 53 s, sagittal orientation, a field of view of 160 × 240 × 256 mm with an isotropic voxel resolution of 1 mm^3, TR = 2300 ms, TE = 2.98 ms, TI = 900 ms, flip angle = 9°. Task-free T2*-weighted echoplanar fMRI scans were acquired with an acquisition time = 8 min 06 s, axial orientation with interleaved ordering, field of view = 230 × 230 × 129 mm, matrix size = 92 × 92, effective voxel resolution = 2.5 × 2.5 × 3.0 mm, TR = 2000 ms, TE = 27 ms, for a total of 240 volumes.

2.3. Structural MRI processing

MP-RAGE scans for both timepoints for a given subject were registered to one another using the symmetric diffeomorphic registration incorporated in the serial longitudinal anatomical MRI package in SPM12 (Ashburner and Ridgway, 2012). This procedure is optimized for longitudinal analysis by correcting for intensity inhomogeneities and creating an average T1 image for each subject, avoiding asymmetric bias that can result from using a particular timepoint (e.g. the baseline image) as the reference image. Default parameters were used for warping regularization and bias regularization. Jacobian determinant and divergence maps were produced that represent the amount of longitudinal brain contraction and expansion. We then applied unified segmentation to the average T1 images (Ashburner and Friston, 2005) with light regularization, a 60 mm bias FWHM cutoff, and Gaussians per tissue type of [2,2,2,3,4,2]. Gray and white tissue segments smoothed with an 8 mm FWHM Gaussian kernel, then multiplied by the divergence deformation maps and scaled by each subject's interscan interval in order to quantify local volume tissue changes over the longitudinal duration of the study. These images were deformed to the standard SPM tissue probability maps using DARTEL with linear elastic regularization and default parameters for the number of inner iterations, regularization parameters, and time steps.

Baseline structural MRI differences were assessed by comparing gray or white matter smoothed, modulated tissue maps using a two-sample *t*-test with covariates for age, sex, and total intracranial volume. Both gray and white matter voxelwise maps were thresholded at two levels of stringency: a liberal level at a height threshold of $p < 0.001$ and an extent threshold of $p < 0.05$, family-wise error (FWE) corrected; and a conservative level, with a correction for a joint height/extent threshold of $p < 0.05$, FWE corrected.

Longitudinal structural MRI differences were determined in the same fashion, performing a two-sample *t*-test on the longitudinal divergence maps multiplied by either the gray or white matter tissue map, with covariates for age, sex, interscan interval in days, and total intracranial volume. This statistical analysis of the change maps was chosen rather than a linear mixed effects model with multiple longitudinal measurements because the serial VBM pipeline performs a single tissue segmentation on the average image. This process is less variable than when performing independent segmentations on separate timepoint maps (Ridgway et al., 2015). Longitudinal structural MRI correlations with PSPRS were assessed using a multiple regression with VBM change maps as the independent variable, PSPRS baseline and PSPRS change as the dependent variables, and covariates for age, sex, interscan interval, and total intracranial volume. An interaction term for PSPRS baseline x PSPRS change was considered but was not significant so was removed from the model. The resultant statistical maps were thresholded at a height threshold of $p < 0.001$ and an extent of $p < 0.05$, FWE corrected. Longitudinal atrophy-clinical correlation maps were also corrected with a height threshold of $p < 0.001$ and an extent of $p < 0.05$, FWE corrected. No clusters survived thresholding at the most conservative joint height/extent of $p < 0.05$, FWE-corrected level.

2.4. Functional MRI processing

For each fMRI scan, the first five volumes were discarded. SPM12 (http://www.fil.ion.ucl.ac.uk/spm/software/spm12/) and FSL (where explicitly specified; http://fsl.fmrib.ox.ac.uk/fsl) software was used for subsequent fMRI preprocessing. The remaining 235 volumes were slice-time corrected, realigned to the mean functional image and assessed for rotational and translational head motion. Volumes were next co-registered to the MP-RAGE image, then normalized to the standard MNI-152 healthy adult brain template using SPM segment, producing MNI-registered volumes with 2 mm^3 isotropic resolution. These volumes were spatially smoothed with a 6 mm radius Gaussian kernel and temporally bandpass filtered in the 0.008–0.15 Hz frequency range using fslmaths. Nuisance parameters in the preprocessed data were estimated for the CSF using a mask in the central portion of the lateral ventricles and for the white matter using a mask of the highest probability cortical white matter as labeled in the FSL tissue prior mask. Additional nuisance parameters included the 3 translational and 3 rotational motion parameters, the temporal derivatives of the previous 8 terms (WM/CSF/6 motion), and the squares of the previous 16 terms (Satterthwaite et al., 2013). All subjects had maximum relative head motion < 3 mm, maximum relative rotation < 3°, and the maximum number of motion spikes (relative motion > 1 mm) < 10% of the total number of frames.

Two complementary approaches were taken for assessment of functional connectivity: a whole brain analysis of whole brain weighted degree, and a targeted analysis of a disease-targeted intrinsic connectivity network anchored in the rMT. To calculate whole brain weight degree maps, we first downsampled the preprocessed tf-fMRI volumes to 4mm^3 resolution in order to make the problem more computationally tractable. We masked the images to a custom gray matter mask compiled from thresholded regional probability maps from the Harvard-Oxford atlases (cortical, subcortical, brainstem) and the FSL FLIRT cerebellar atlas. The timeseries from each voxel was partially correlated with every other voxel in a pairwise fashion, controlling for the 32 nuisance parameters, to produce a 23,714 × 23,714 matrix. For each voxel, the unthresholded columnwise sum was taken to determine the whole brain weighted degree (referred to as WBD henceforth), which was then stored for that voxel in a three dimensional image.

Network connectivity in the rMT network was determined by taking regional masks for the 27 nodes comprising the rMT-anchored network, applying them to a given subject's preprocessed tf-fMRI data to extract regional mean timeseries, and partially correlating those timeseries in a pairwise fashion again controlling for the 32 nuisance parameters to obtain the 27 × 27 connectivity matrix. Each matrix was then r-to-Z transformed. To assess the healthy network graph theoretical properties, the mean connectivity matrix from both timepoints of all 20 HC subjects was taken and analyzed with the Brain Connectivity Toolbox (https://sites.google.com/site/bctnet/). We were interested in determining which subsets of nodes in this network were most tightly coupled with one another to form sub-networks or “modules”, based on the expectation that these modules would correspond to particular intrinsic connectivity networks supporting different cognitive and behavioral functions (Power et al., 2011). The modular structure of the network was determined by calculating the Louvain modularity on the unthresholded group matrix 1000 times and finding the partition that balanced the criteria of being among the most frequent solutions and maximizing the modularity value of Q, the quality of the partitioning (Rubinov and Sporns, 2011). We labeled the winning partition as the fixed “community index” and performed all subsequent modularity analysis using this index. For each subject, for each node, we determined two related quantities: the intramodular connection strength, the mean connectivity of each node to every other node within its module; and the intermodular connection strength, the mean connectivity to the remaining extramodular nodes.

We compared the spatial overlap of the 27 rMT nodes with known intrinsic connectivity networks as defined by Yeo and colleagues (Yeo

et al., 2011). For each ROI, we found which of the 7 ICNs it had the greatest overlap with. The "Ventral Attention" network we refer to here as the salience network based on the significant similarity between them (Seeley et al., 2007).

For all functional connectivity (FC) analyses, we determined baseline differences between PSP-S and HC using a two-sample *t*-test with covariates for age and sex. Longitudinal analyses were performed using linear mixed effects models. For voxelwise statistics on WBD maps, AFNI's 3dLME program was used (http://afni.nimh.nih.gov/pub/dist/doc/program_help/3dLME.html) (Chen et al., 2013). For nodewise and edgewise statistics from the rMT graph theory analysis, the 'fitlme' program in MATLAB was used (http://www.mathworks.com/help/stats/fitlme.html). The linear mixed effects model used to determine different longitudinal FC change in PSP-S vs. HC included fixed effects for group, timepoint, group X timepoint interaction, age, sex, and interscan interval and a random intercept for subject identity. Prediction of imaging change based on baseline PSPRS was modeled as a linear regression with the (time 1 – time 2) imaging measure as the independent variable and baseline PSPRS, baseline age, and sex as the dependent variables. The model for determining FC change associated with clinical change included only PSP-S subjects and had fixed effects for PSPRS baseline score, PSPRS time 1 to time 2 change (or delta), the PSPRS baseline X delta interaction (representing change that is greater in patients with greater clinical impairment at baseline *and* greater clinical worsening from baseline to follow-up), age, sex, interscan interval, and a random effect for subject identity. This model was only assessed for PSP-S subjects because the bimodal distribution PSPRS scores in a group of patients (with high nonzero values) and controls (with all zero values) would prevent accurate linear fitting of PSPRS to FC values. WBD voxelwise maps were corrected for multiple comparisons using a height threshold of $p < 0.01$, uncorrected and an extent of $p < 0.01$, uncorrected. This relatively liberal threshold was used because we interpreted WBD secondarily to rMT network connectivity. WBD two group comparisons were also assessed after gray matter atrophy correction, using the subject's baseline smoothed/normalized/normalized gray matter tissue maps as voxelwise covariates in the Biological Parametric Mapping toolbox (Casanova et al., 2007). Statistical tests of rMT network FC measures were corrected for multiple comparisons using false discovery rate (FDR) correction at the module level ($n = 6$), node level ($n = 27$), or edge level ($n = 351$). To confirm that the between-group differences in node weighted degree at baseline were not an artifact of a relatively small sample size in a parametric test, we also tested between group differences using a permutation test. In this procedure we 1) took the raw value of weighted degree for a given node across all subjects, 2) covaried out the effect of age, sex, and global gray matter atrophy (see below), 3) found the true difference in means between PSP patients and controls, randomly shuffled the values, 4) found the pseudo difference in means between the two groups, 5) repeated the shuffling 5000 times, and 6) counted the percentage of trials in which the difference in pseudo means excluded the difference in true means. In order to justify the use of parametric mixed effect models, we tested the normality of the edgewise FC value distribution in both patients and controls using a Shapiro-Wilk test (Ghasemi and Zahediasl, 2012). Both groups had normally distributed FC values after the r-to-Z transform (PSP-S: $p = 0.90$, HC: $p = 0.59$).

Statistical models of all rMT network measures were assessed both without and with global atrophy correction, where global atrophy for each subject was defined as the ratio of gray matter volume to total intracranial volume. There are a number of different strategies that can be used for atrophy correction, including 1) correction atrophy in the node/nodes under consideration, 2) using a landmark-based correction, such as midbrain volume, or 3) using a global atrophy correction. We opted for a global atrophy correction strategy because our patients showed significant brain-wide atrophy, and in order to make the correction comparable across all of our tests.

Network diagrams were rendered using NetworkX (https://networkx.github.io/), bar plots and line plots were created with Seaborn (https://seaborn.pydata.org/), and brain overlay images were produced with Nilearn (http://nilearn.github.io/).

3. Results

3.1. Patients with PSP-S show variable rates of clinical progression

Patients were first assessed for clinical severity at baseline and follow up using the PSPRS to assess the degree of heterogeneity in clinical progression. At baseline, patients had mild to moderate PSPRS baseline scores (mean = 27.6 ± 10.6). Progression rates were variable (mean change = 6.3 ± 7.8).

3.2. The healthy rMT-anchored intrinsic connectivity network is modular and has hubs in the thalamus, basal ganglia, paracingulate and posterior midcingulate

We previously identified reductions in rMT-anchored ICN connectivity in PSP-S and correlated these reductions with disease severity (Gardner et al., 2013). Here, we more deeply characterized the rMT ICN's modular composition to understand if the disease process preferentially targeted specific subnetworks or hub regions. Using the 27 nodes comprising the rMT network as defined previously, we estimated the group average rMT functional connectivity matrix from the healthy controls at time 1 in this study. We applied a modularity detection algorithm to this matrix and identified three modules – a medial posterior-parietal module, Module 1 (Fig. 1, blue regions); a prefrontal-paralimbic module, Module 2 (Fig. 1, red regions); and a subcortical-brainstem module, Module 3 (Fig. 1, green regions). Hub nodes were identified based on the product of their intramodular and intermodular connectivity strength. The main hubs were the posterior midcingulate cortex (pMCC; Module 1), paracingulate (Module 2), and thalamus (Module 3) (Fig. 1D, upper right). The pMCC-thalamus connection was the primary interface between modules 1 and 3, while the paracingulate-basal ganglia connection linked modules 2 and 3. The main connector regions linking modules 1 and 2 were the pMCC, precuneus, paracingulate, anterior cingulate, and middle frontal gyrus.

We next compared the spatial correspondence between the 2 cortical modules and known cortical intrinsic connectivity networks defined by Yeo and colleagues (Yeo et al., 2011). Module 1 nodes primarily belonged to the posterior aspect of the default mode network (retrosplenial cortex and posterior midcingulate) and dorsal attention network (precuneus) and module 2 nodes to the executive control network (middle frontal gyrus, paracingulate), salience network (insula, supramarginal gyrus), and anterior default mode network (pregenual anterior cingulate). Module 3 contained all subcortical, brainstem, and cerebellar nodes, regions that were not included in the comparison to the cortical-only networks from the Yeo study.

3.3. PSP-S baseline deficits are concentrated in hub regions of the rMT-anchored ICN

At baseline, PSP-S patients demonstrated substantial atrophy and functional connectivity reductions compared to controls. Within the rMT network, mean FC strength was lower ($t = 4.17$, $p = 0.0003$ without atrophy correction/2.67, $p = 0.01$ with atrophy correction). Intermodular FC strength was significantly reduced ($p < 0.05$, FDR corrected without atrophy correction) for module 1–module 2 ($t = 4.43$ without AC/3.05 with AC) and module 2–module 3 ($t = 3.88/2.66$), while intra-module strength was reduced for modules 2 ($t = 2.98/2.16$) and 3 ($t = 4.28/2.51$) (Fig. 2). All of these inter/intramodular connections were also significantly lower in patients with PSP-S using a non-parametric test ($p < 0.05$, FDR corrected). All of these reductions were tested for longitudinal consistency in a mixed effect model with terms for diagnosis (PSP-S or HC) and timepoint (baseline or follow-

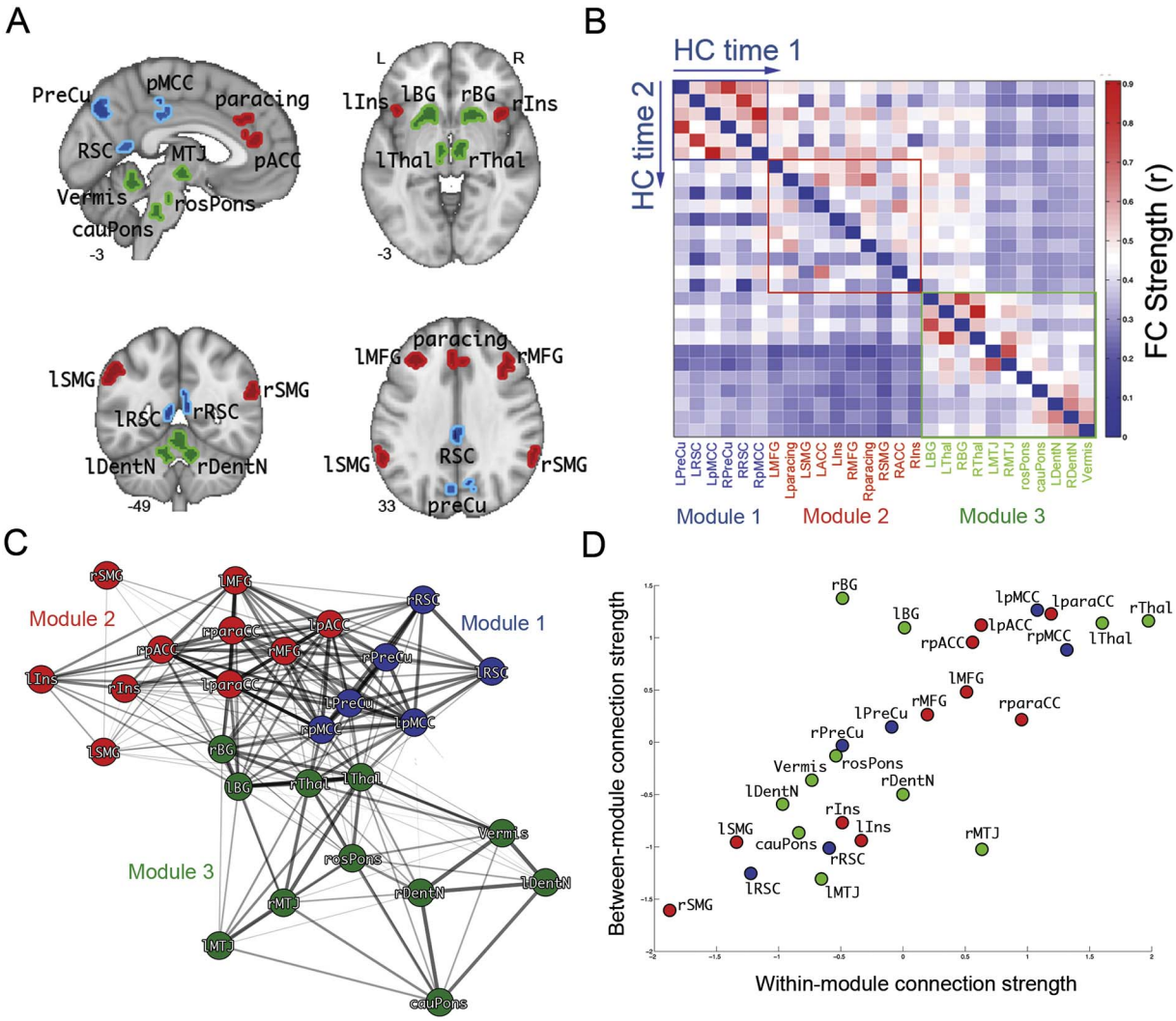

Fig. 1. Rostral midbrain tegmentum-anchored intrinsic connectivity network configuration in healthy control subjects. A. The 27 regions comprising the network, colored according to their membership in Module 1 (blue), Module 2 (red), or Module 3 (green). B. Group mean functional connectivity matrix at baseline (upper triangle) and longitudinal follow-up (lower triangle). Nodes are ordered according to module membership. C. Spring-embedded graph illustrates the modular connectivity of the network. D. Scatter plot of each node's within-module functional connectivity strength vs. its between-module functional connectivity strength. The nodes with the highest combination of intramodular and intermodular connectivity, the hubs, are located in the thalamus, paracingulate cortex, and posterior midcingulate cortex. The other major nodes with high intermodular connectivity, the connector hubs, are the basal ganglia (Module 3 to Module 2) and anterior cingulate cortex (Module 2 to Module 1). PreCu: precuneus, RSC: retrosplenial cortex, pMCC: posterior midcingulate cortex, MFG: middle frontal gyrus, paracing: paracingulate cortex, SMG: supramarginal gyrus, pACC: pregenual anterior cingulate cortex, Ins: insula, BG: basal ganglia, Thal: thalamus, MTJ: mesothalamic junction, rosPons: rostral pons, cauPons: caudal pons; DentN: dentate nucleus, Vermis: cerebellar vermis. (For interpretation of the references to color in this figure legend, the reader is referred to the web version of this article.)

up). The main effect of diagnosis was significant ($p < 0.013$, FDR corrected) for module 1–2 ($t = 4.52$ without AC/3.23 with AC), 2–3 ($t = 4.48/3.49$), 2–2 ($t = 3.31/2.55$), and 3–3 ($t = 4.43/3.10$).

In line with the global reductions in rMT FC, 14 out of 27 nodes showed reduced weighted nodal degree at baseline ($p < 0.05$, FDR corrected without AC; * indicates FDR significance with AC). The most disconnected regions at baseline were the left basal ganglia (BG) ($t = 5.04$ without AC/3.39* with AC), left paracingulate ($t = 4.86/3.86$*), right middle frontal gyrus (MFG; $t = 4.23/3.29$*), left insula ($t = 3.96/2.66$*), left mesothalamic junction (MTJ; $t = 3.86/2.17$), right insula ($t = 3.72/2.31$), right MTJ ($t = 3.68/1.80$), left posterior midcingulate (pMCC; $t = 3.65/2.01$), left MFG ($t = 3.60/2.79$*), left precuneus ($t = 3.55/2.48$), right dentate nucleus ($t = 3.53/2.10$), right thalamus ($t = 3.48/2.21$), right BG ($t = 3.47/2.30$), and left thalamus ($t = 3.44/2.24$). All of these nodes also had significantly lower weighted degree in patients with PSP-S when tested with a non-parametric test ($p < 0.05$, FDR corrected). Furthermore, every one of these regions showed consistently lower weighted degree based on the longitudinal mixed effect model main effect of diagnosis (all $p < 0.05$, FDR corrected with or without AC).

The most severely reduced edge weights at baseline (FDR corrected $p < 0.05$) were left paracingulate-[right BG ($t = 4.66$ without AC/4.32 with AC)], left thalamus-[right thalamus ($t = 5.23/4.43$)], and left BG-[right thalamus ($t = 4.54/3.50$), left MTJ ($t = 4.44/3.07$), right dentate nucleus ($t = 4.70/3.69$)], all of which were consistently reduced longitudinally (all longitudinal mixed effect model main effects of diagnosis survived Bonferroni correction). In total, 33% of edges (117 out of 351; 10% with AC, 35/351) showed baseline deficits that were consistently lower longitudinally, consistent with the observed deficits in global, modular, and nodal FC.

To complement the targeted analysis of FC in the rMT network, we assessed brain-wide FC patterns in order to understand the focality of FC deficits in PSP-S. Regions with the most severe whole brain weighted degree reductions overlapped considerably with the rMT network, including the anterior and paracingulate cortex, the caudate head, retrosplenial cortex, midcingulate cortex, and middle frontal gyrus

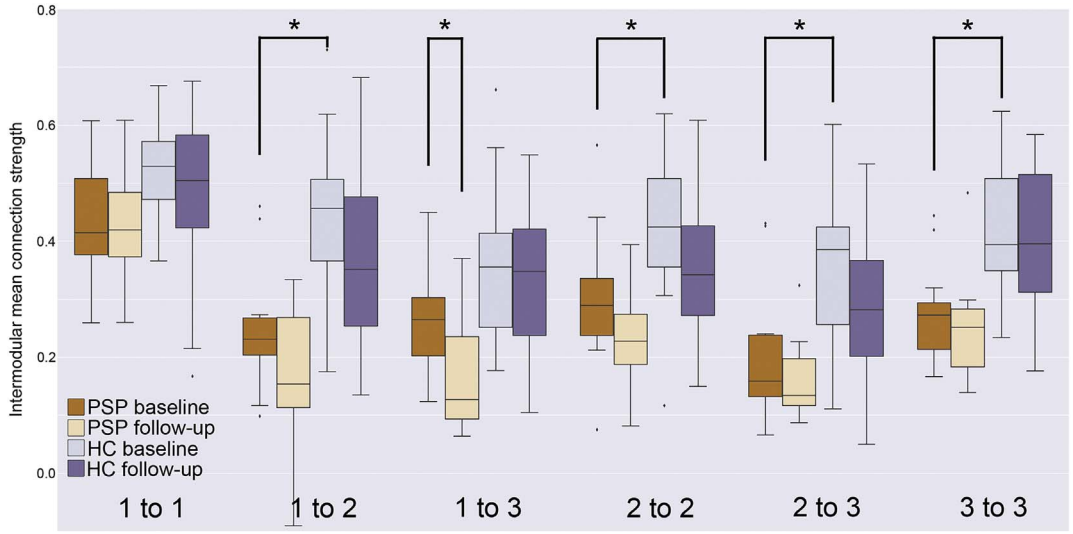

Fig. 2. Intra and intermodular mean functional connectivity strengths at baseline and follow-up for PSP-S patients and healthy controls. Significant baseline reductions in PSP-S patients with respect to controls (*, $p < 0.0083$) were detected for module 1 to module 2, intra-module 2, module 2 to module 3, and intra-module 3. A significant longitudinal decline in PSP-S patients was found for module 1 to module 3.

(Fig. 3A; height $p < 0.01$/extent $p < 0.01$). We measured these FC reductions after correcting for gray matter atrophy in each voxel, which helps reveal where reduced FC is observed independent of structural alterations. After atrophy correction, the strongest reductions were largely confined to the same regions found in the non-atrophy-corrected map, with peaks in the right precuneus, insula, inferior frontal gyrus, and middle frontal gyrus (Table S1).

Structural MRI revealed widespread atrophy in gray and white matter (Fig. 3B; two levels of correction: height $p < 0.05$ FWE/extent $p < 0.05$ FWE and height $p < 0.001$/extent $p < 0.05$ FWE; Table S2). Lower gray matter volume was found in the supplementary motor area (SMA), paracingulate, precuneus, dorsal and ventral medial prefrontal cortex. White matter atrophy was detected in the mesothalamic junction, inferior frontal-occipital fasciculus, and corona radiata.

3.4. PSP-S longitudinal declines follow a midbrain-to-posterior cortical trajectory

Longitudinal declines in rMT network connectivity were assessed in two ways: 1) in a patients-only models, to determine if declines are large enough to be a reliable outcome measure in a clinical trial, and 2) with patients and controls in a combined group model, to validate the

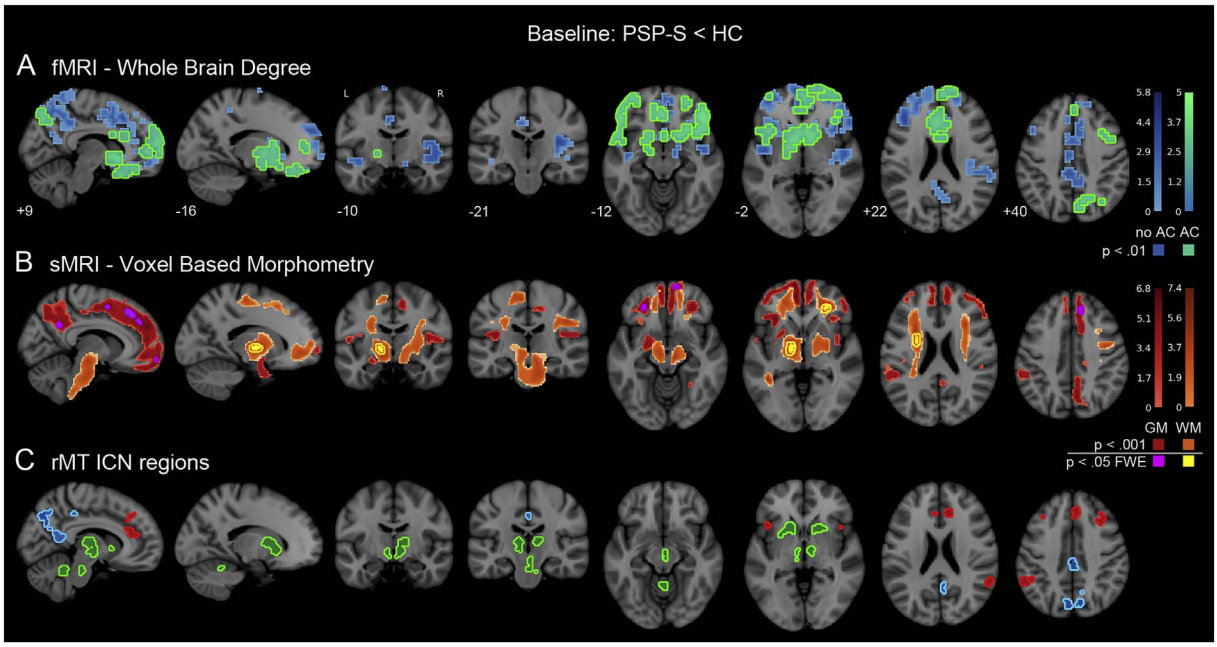

Fig. 3. Baseline differences in whole brain functional connectivity and tissue volume. A. Whole brain weighted degree deficits in PSP-S with respect to healthy controls, shown with and without correction for voxelwise gray matter volume (green and blue, respectively). The strongest reductions were found in the right inferior frontal gyrus, insula, middle frontal gyurs, precuneus, and caudate. Voxels that showed reduction after atrophy correction (AC; green) were nearly a perfect subset of voxels showing reduction with no AC (blue) and are therefore shown superimposed on top of the no AC map. B. Voxel based morphometry volume reductions in PSP-S were apparent in gray matter areas including the paracingulate cortex, supplementary motor area, and precuneus; and white matter areas including the mesothalamic junction and corona radiata. C. The 27 rMT-ICN regions shown for anatomical correspondence with functional and structural deficits. AC: atrophy correction. GM: gray matter. WM: white matter. Colorbars indicate t-statistic range. (For interpretation of the references to color in this figure legend, the reader is referred to the web version of this article.)

disease-specificity of FC changes. The patient-only model, showed a significant reduction in module 1–module 3 connectivity (PSP-only mixed model main effect of time, $t = -3.33$ without AC/-3.34 with AC, FDR corrected $p < 0.05$, Fig. 2), indicating progressive disconnection between a posterior cortical and a subcortical/brainstem module that remained intact at baseline. However, the combined two-group model of intermodular FC decline only found a trend for module 1–module 3 6-month decline ($t = 2.04/2.04$, $p = 0.04$, effect size = 0.50), suggesting that FC change would not be a sufficient biomarker for disease diagnosis. The FC declines for the other modular intra/interconnections were less discriminative (module 1–module 1: effect size d = 0.22; 1–2: d = 0.04; 2–2: d = 0.09; 2–3: d = 0.31; 3–3: d = 0.01). In the PSP-only model, a probe of edge-wise contributions to module 1–module 3 uncoupling revealed significantly reduced FC between right pMCC-right MTJ ($t = -3.97/-4.15$, FDR corrected $p < 0.05$). Thus the progressive intermodular disconnection and progressive isolation of the subcortical/brainstem module was driven primarily by reduced connectivity between the MTJ and pMCC. When assessing voxelwise whole brain degree, we found no evidence of accelerated longitudinal changes in PSP with respect to control subjects.

We next assessed whether steeper rates of longitudinal atrophy were present in the patients with PSP-S in comparison to healthy controls, despite variable rates of clinical progression. Compared with the rates of regional gray and white matter volume loss in controls, patients with PSP-S showed greater longitudinal atrophy in perirolandic cortex and the underlying white matter, concentrated in the precentral gyrus (Fig. 4B; height $p < 0.001$/extent $p < 0.05$ FWE; mean effect size = 1.41; Table S3). Subcortically, progressive atrophy was concentrated in the midbrain and pallidum.

3.5. PSP-S clinical worsening accompanies distributed frontal cortical network isolation

An alternative strategy for monitoring disease-related brain change is to examine changes that correlate with clinical severity, rather than changes that occur regardless of clinical progression. We investigated this by looking at two different imaging-clinical relationships: 1) longitudinal brain changes that correlate with the level of baseline clinical severity and 2) longitudinal brain changes that correlate with the degree of longitudinal clinical worsening. We first examined FC-clinical relationships in the rMT network using a longitudinal linear mixed effects model. Elevated baseline PSPRS predicted subsequent decoupling between Module 1–Module 2 ($t = 3.46/3.86$, FDR corrected $p < 0.05$). PSPRS longitudinal increases were correlated with decreasing connectivity within Module 2 ($t = -3.00/-2.45$, FDR corrected $p < 0.05$). We did not find a significant relationship between baseline levels of FC deficit and subsequent PSPRS change. We also found no significant relationships between voxelwise whole brain degree maps and PSPRS baseline, change, or the baseline x change interaction.

In patients with higher baseline PSPRS, we observed greater subsequent longitudinal gray matter atrophy in the perirolandic cortex, supplementary motor area, midcingulate cortex, precuneus, thalamus, and midbrain, (Fig. 5, red-yellow; height $p < 0.001$/extent $p < 0.05$ FWE; Table S4). White matter correlations were present in the corona radiata, superior longitudinal fasciculus, and superior cerebellar peduncle (Fig. 5, blue; height $p < 0.001$/extent $p < 0.05$ FWE; Table S4). No correlations between VBM change and PSPRS change were detected, nor did we find a relationship between baseline levels of structural atrophy and subsequent PSPRS change.

4. Discussion

Here we report that, over 6 months, patients with mild to moderate PSP-S show progressive atrophy and loss of functional connectivity, extending beyond deficits present at baseline. At baseline, FC was broadly reduced in regions comprising the rMT network. The most severe deficits were in hub regions linking the subcortical-brainstem and prefrontal-paralimbic modules. Baseline structural atrophy involved overlapping brainstem, subcortical, frontal, and parietal areas. Longitudinally, patients showed the most severe FC declines between the subcortical-brainstem module and the medial parietal module. Group-wide longitudinal structural atrophy was found in the midbrain, pallidum, perirolandic cortex, and superior cerebellar peduncle, and was steeper in patients at a more advanced clinical stage.

4.1. Baseline functional connectivity deficits in PSP-S target rMT network hubs

Functional disconnection of brainstem, subcortical, and cortical functional modules results in isolation of these networks from one another. We characterized the functional network modularity of the rMT-anchored network in healthy controls and identified 3 modules: a medial parietal module (Module 1, anchored by the posterior midcingulate cortex), a prefrontal-paralimbic module (Module 2, anchored by the anterior paracingulate cortex), and a subcortical-brainstem module (Module 3, anchored by the basal ganglia and thalamus). A previous study had found PSP-S FC reductions in all 3 of these modules, most prominently in regions which we now identify as the prefrontal-paralimbic module (Gardner et al., 2013). In the current study, patients at baseline showed most impairment within and between Modules 2 and 3, with the strongest effects concentrated in hub nodes in the paracingulate cortex and basal ganglia. Graph theoretical analysis of this network in healthy controls revealed that the Module 2–Module 3 connections via the basal ganglia were the primary subcortical-frontal lobe interface. Patients with PSP-S typically have deficits in motor and cognitive inhibition, dependent on common circuitry in a control network including the subthalamic nucleus, pallidum, striatum, inferior frontal gyrus, preSMA, and dorsolateral prefrontal cortex (Aron and Poldrack, 2006; Jahanshahi et al., 2015). Impaired FC in these regions likely reflects degradation of this system and disrupts inhibitory control in PSP-S.

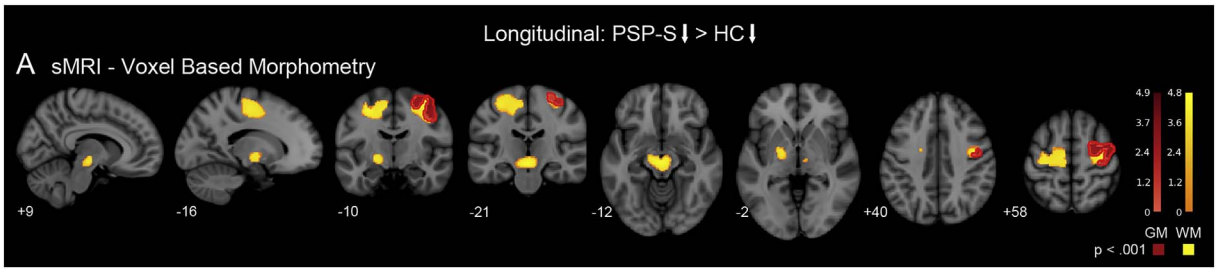

Fig. 4. Group-level longitudinal atrophy in PSP-S with respect to healthy controls. A. Longitudinal atrophy compared to controls was identified in the perirolandic gray and white matter, pallidum, and midbrain. GM: gray matter. WM: white matter. Colorbars indicate t-statistic range.

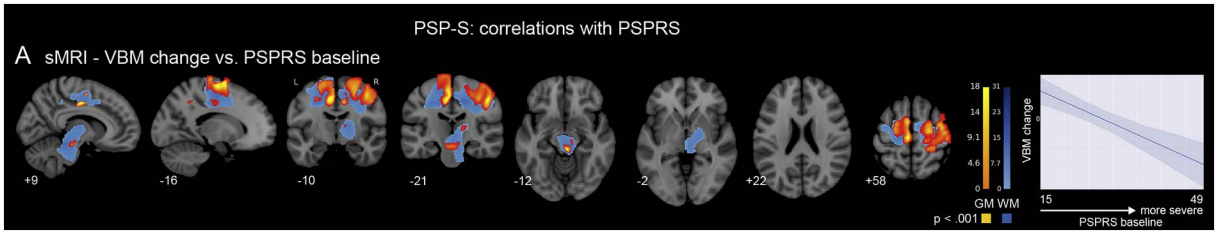

Fig. 5. Longitudinal atrophy that correlates with clinical worsening. A. Areas where gray or white matter longitudinal atrophy negatively correlate with PSPRS baseline score included the perirolandic cortex, supplementary motor area, midcingulate cortex, thalamus, midbrain, corona radiata, superior longitudinal fasicuclus, and superior cerebellar peduncle. Line plot shows mean VBM change (longitudinal atrophy) in the gray matter map as a function of increasing PSPRS baseline. GM: gray matter. WM: white matter. Colorbars indicate t-statistic range. (For interpretation of the references to color in this figure, the reader is referred to the web version of this article.)

4.2. Functional connectivity levels at baseline do not predict subsequent clinical change

The framework we used in this study to assess longitudinal brain change with respect to clinical change specified four types of brain-clinical relationship: 1) biomarker change anticipating clinical change, 2) biomarker and clinical change progressing in locked step, 3) clinical change anticipating biomarker change, and 4) biomarker change independent of clinical change (Table 2). We did not detect any baseline biomarker levels that anticipated clinical change, addressing our study's open question about the relationship between baseline clinical status and subsequent longitudinal neuroimaging. The evaluation of functional neuroimaging biomarkers is most mature in Alzheimer's Disease, where evidence suggests that task-free fMRI connectivity abnormalities appear in cognitively normal at-risk individuals who do not yet have amyloid deposition (Jones et al., 2016; Machulda et al., 2011; Sheline et al., 2010), structural atrophy, or cognitive impairment (Jack et al., 2013). Longitudinal fMRI studies in AD have detected progressive decline in functional connectivity in subsystems of the default mode network and accompanying cognitive declines (Damoiseaux et al., 2012). To date, however, no tight link has yet been demonstrated between baseline tf-fMRI connectivity impairments and near-term subsequent cognitive decline in a within-subject longitudinal study. Given that all patients in this study were symptomatic at baseline and that the strongest detected effects were correlations between clinical severity (PSPRS baseline/change) and FC *change*, it is possible that the most substantial FC changes may occur before the onset of symptoms and that the inter-subject variations in baseline FC level are less sensitive to subsequent clinical decline than are within-subject FC longitudinal changes. Longer-term follow-up studies are needed to address this important possibility.

4.3. Frontal functional connectivity reductions relate to clinical impairment

Longitudinal FC declines were correlated with simultaneous PSPRS change, regardless of disease stage at baseline. Within the rMT network, declines in intra-Module 2 functional connectivity were coupled with worsening PSPRS. Module 2 was the most extensive, encompassing subnetworks corresponding to multiple ICNs including the executive control, salience, and anterior default mode networks. The PSPRS primarily scores motor functioning, raising the question of why PSPRS worsening would correlate with decreases in Module 2 functional connectivity, a network that may appear primarily "cognitive". However, frontal lobe dysfunction can result in co-incident executive and motor impairments, particularly gait disturbances and falls (Segev-Jacubovski et al., 2011) (Leisman et al., 2016). The multi-network, distributed nature of this module makes it more likely that FC loss will be protracted across disease stages.

Patients in this study showed deficits in executive functions at baseline, including working memory (digit span), processing speed (trails), and verbal fluency (Boston naming test, letter fluency, semantic fluency). The primary system supporting these processes is the fronto-parietal executive control network (Hedden and Gabrieli, 2010; Seeley et al., 2007). The dorsolateral prefrontal portion of the executive control network is a working memory locus (Levy and Goldman-Rakic, 2000), represented by the middle frontal gyrus node in this study. Here we found that the left and right MFG had impaired FC at baseline. A complementary node of the executive control network in the dorsal medial frontal cortex is critical for response selection (Simmonds et al., 2008), represented here by the paracingulate and ACC nodes. These nodes were also the main cortical interface to the "basal ganglia" node which covered the caudate and anterior putamen, both of which are known to participate in fronto-parietal control/attention systems (Choi et al., 2012; Greene et al., 2014). Coincidentally, apathy is associated with impaired communication between the prefrontal cortex and basal ganglia (Levy and Dubois, 2006). Apathy is the most consistent neuropsychiatric symptom in PSP-S, appearing in up to 91% of subjects (Bruns and Josephs, 2013; Litvan et al., 1996), and routinely accompanies executive deficits in neurodegenerative disease (McPherson et al., 2002). In PSP-S, more severe apathy correlates with reduced integrity in frontal white matter pathways including the superior longitudinal and uncinate fasciculi (Agosta et al., 2014), both of which show atrophy at baseline in the current study. Thus, both the baseline cognitive/behavioral symptoms and clinical progression observed in this study can be linked to the deficits in frontal lobe (ie Module 2) connectivity.

Table 2
Summary of neuroimaging biomarker-clinical relationships by type of relationship and type of imaging modality. *: results were significant in a patient-only model. rMT ICN: rostral midbrain tegmentum intrinsic connectivity network.

Type of biomarker-clinical longitudinal relationship	rMT ICN Module tf-fMRI	Voxel based morphometry
1–Biomarker baseline deficit before clinical change	None detected	None detected
2A–Biomarker change locked with clinical change	Module 2–Module 2	None detected
2B–Biomarker change locked with clinical change, more so for high PSPRS baseline + change patients	None detected	None detected
3–Baseline clinical severity correlated with biomarker change	Module 1–Module 2	Perirolandic cortex, midcingulate cortex, supplementary motor area, precuneus, thalamus, midbrain, superior cerebellar peduncle
4–Biomarker change independent of clinical change	Module 1–Module 3*	Perirolandic cortex, pallidum, and midbrain

4.4. Baseline levels of clinical severity anticipate subsequent atrophy and functional connectivity decline in already-impaired regions

Baseline clinical severity predicted subsequent decoupling between Module 1 (precuneus) and Module 2 (anterior cingulate), a connection that was already impaired at baseline. Greater baseline severity also correlated with higher subsequent rates of atrophy in the perirolandic cortex, supplementary motor area, midcingulate cortex, precuneus, thalamus, and midbrain (Fig. 5). A higher rate of decline in more clinically impaired patients indicates a non-linear rate of biomarker change that accelerates as the disease progresses (Josephs et al., 2013). The strongest PSPRS-biomarker correlations involved atrophy and rMT connectivity, both of which included earlier stage regions (subcortical and prefrontal) and later stage regions (posterior frontal and parietal). This may be evidence for staggered progression, where the most vulnerable early-stage regions continue to decline while late-stage regions begin to accelerate their decline.

4.5. Longitudinal atrophy and functional connectivity loss appear along a midbrain-to-posterior cortical pathway regardless of clinical progression

Longitudinal declines independent of clinical severity or progression also occurred in patients with PSP-S. Group-wide FC declines were observed between Module 1 and Module 3 (Fig. 2). The decline of FC between networks showing no significant baseline impairments supports a staged process of disease progression, validating our study's primary hypothesis. Importantly, this change was not significant in the combined model with PSP-S and controls, only appearing as a trend ($t = 2.04$, $p = 0.04$). This may be due to the limited sample size in this study and needs to be followed up on in a larger future study. Simultaneous atrophy was detected in perirolandic cortex, midbrain, and pallidum. This posterior frontal atrophy and declining parietal FC is reminiscent of stages 2 and 3 of tau pathology observed post-mortem (Williams et al., 2007), the stages that might be expected in the mild-to-moderate severity cohort we studied. The connections that weakened most were between the mesothalamic junction and posterior midcingulate cortex. The posterior midcingulate cortex contains motor areas which participate in skeletomotor responses via convergent projections with the primary motor cortex to the striatum (Vogt et al., 2003). The collective picture that emerges is an earlier stage of subcortical-frontal cortical disturbance and subsequent disease progression along a subcortical-posterior cortical axis. Dutt and colleagues recently reported a similar pattern of baseline subcortical-frontal atrophy in patients with PSP-S and subsequent longitudinal atrophy over one year in subcortical and posterior cortical areas (Dutt et al., 2016). Patients with PSP-S are known to exhibit an executive prodrome involving mental rigidity, multitasking deficits, and apathy, with motor symptoms manifesting soon thereafter (Kertesz and McMonagle, 2010). The baseline executive deficits in our cohort did indeed accompany impaired baseline connectivity and atrophy concentrated in Module 2 and 3. What remains unclear is why longitudinal intra-Module 2 FC reductions were correlated with simultaneous clinical worsening on the PSPRS, while Module 1–Module 3 FC reductions were not. One possibility is that among rMT network nodes, Module 2 FC is most tightly linked to functions measured by the PSPRS, given that all of the significant rMT FC/clinical correlations found in this study involved Module 2. We did observe longitudinal atrophy in the midbrain, an area that showed baseline FC deficits in the rMT network. However, other later stage regions like the perirolandic cortex showed longitudinal atrophy without baseline FC deficits. One limitation of the rMT network is its lack of posterior frontal nodes where longitudinal atrophy was most pronounced. On the other hand, given that WBD did not detect any significant group-wide FC declines in patients, it may be too coarse of a measure to capture subtle network-specific FC deficits that precede structural atrophy. Future studies should consider examining FC in a sensory-motor network in addition to those ICNs covered by the rMT network here.

4.6. The role of functional connectivity and structural atrophy as biomarkers in a clinical trial

In clinical trials for PSP, Tideglusib was found to slow rates of atrophy in the whole brain, particularly the parietal and occipital lobes, despite no slowing of clinical progression (Höglinger et al., 2014). Other clinical trials have also failed to slow clinical worsening (Boxer et al., 2014). Based on the findings in this study, we suggest the following considerations for a PSP clinical trial with FC and structural atrophy as outcome measures. First, patients with mild-to-moderate PSPRS scores already showed widespread structural atrophy and reduced FC in subcortical, frontal, and parietal areas.

Second, later stage patients showed steeper rates of atrophy and rMT FC decline in certain regions, while no regions showed higher rates of decline in earlier stage patients. Thus, these atrophy and FC measurements may be more effective as later-stage biomarkers, when rates of change appear to be higher. Third, patients showed variable rates of clinical progression that were locked with simultaneous FC decline and atrophy, primarily in prefrontal-paralimbic regions. Fourth, Module 2 is likely to show the greatest clinical sensitivity across disease stages, based on a) the Module 2 FC correlations with both PSPRS baseline and change, b) baseline FC deficits in the MFG, paracingulate, and basal ganglia, c) the known executive prodrome in PSP-S, and d) the greater to signal-to-noise ratio of the fMRI BOLD signal in cortical versus brainstem regions (Beissner et al., 2014). Finally, FC levels must be considered in the context of patient medications for motor and behavioral symptoms; in particular, levodopa has previously been shown to increase tf-fMRI connectivity levels in patients with Parkinson's disease and healthy controls (Cole et al., 2013; Simioni et al., 2017) and may partially diminish differences between patients and controls, including those in this study. We limited our effect size calculations to those biomarkers that showed significantly different rates of change in patients and controls, or at least a significant effect of change in patients. Overall, in this sample of patients with mild-to-moderate clinical severity, structural atrophy measurement in the midbrain, pallidum, and perirolandic cortex was most effective for detecting disease-related change. Future studies of very early stage patients with PSP or even healthy subjects at genetic risk for PSP based on a MAPT H1 haplotype (Fogel et al., 2014) and a risk profile based on known risk alleles could monitor FC in vulnerable subcortical and frontal networks to establish the original FC alterations that mark disease onset and evaluate their efficacy as early-stage biomarkers.

Acknowledgements

We are grateful to all patients and caregivers who participated in research. We would like to thank Helen Zhou and Eric Ng for their assistance with data analysis and interpretation.Funding

This study was supported by NIH grants R01AG038791, U54NS092089, P01AG019724, and the Tau Research Consortium.Data sharing

The unthresholded statistical maps for baseline VBM PSP < HC (gray and white matter), baseline whole brain degree PSP < HC, longitudinal VBM PSP > HC (gray and white matter), longitudinal VBM correlations (gray and white matter) with PSPRS, and the 27 rMT network ROIs are available for download at http://neurovault.org/. The rMT network connectivity matrices for patients and controls for both timepoints (total n = 64) are available at http://umcd.humanconnectomeproject.org/umcd/default/browse_studies under the study name “UCSF_MAC_PSP”.

Appendix A. Supplementary data

Supplementary data to this article can be found online at http://dx.doi.org/10.1016/j.nicl.2017.09.008.

References

Agosta, F., Galantucci, S., Svetel, M., Lukić, M.J., Copetti, M., Davidovic, K., Tomić, A., Spinelli, E.G., Kostić, V.S., Filippi, M., 2014. Clinical, cognitive, and behavioural correlates of white matter damage in progressive supranuclear palsy. J. Neurol. 261, 913–924. http://dx.doi.org/10.1007/s00415-014-7301-3.

Aron, A.R., Poldrack, R.A., 2006. Cortical and subcortical contributions to stop signal response inhibition: role of the subthalamic nucleus. J. Neurosci. 26, 2424–2433. http://dx.doi.org/10.1523/JNEUROSCI.4682-05.2006.

Ashburner, J., Friston, K.J., 2005. Unified segmentation. NeuroImage 26, 839–851. http://dx.doi.org/10.1016/j.neuroimage.2005.02.018.

Ashburner, J., Ridgway, G.R., 2012. Symmetric diffeomorphic modeling of longitudinal structural MRI. Front. Neurosci. 6, 197. http://dx.doi.org/10.3389/fnins.2012.00197.

Bak, T.H., Crawford, L.M., Hearn, V.C., Mathuranath, P.S., Hodges, J.R., 2005. Subcortical dementia revisited: similarities and differences in cognitive function between progressive supranuclear palsy (PSP), corticobasal degeneration (CBD) and multiple system atrophy (MSA). Neurocase 11, 268–273. http://dx.doi.org/10.1080/13554790590962997.

Beissner, F., Schumann, A., Brunn, F., Eisenträger, D., Bär, K.-J., 2014. Advances in functional magnetic resonance imaging of the human brainstem. NeuroImage 86, 91–98. http://dx.doi.org/10.1016/j.neuroimage.2013.07.081.

Boxer, A.L., Geschwind, M.D., Belfor, N., et al., 2006. Patterns of brain atrophy that differentiate corticobasal degeneration syndrome from progressive supranuclear palsy. Arch. Neurol. 63, 81–86. http://dx.doi.org/10.1001/archneur.63.1.81.

Boxer, A.L., Lang, A.E., Grossman, M., Knopman, D.S., Miller, B.L., Schneider, L.S., Doody, R.S., Lees, A., Golbe, L.I., Williams, D.R., Corvol, J.-C., Ludolph, A., Burn, D., Lorenzl, S., Litvan, I., Roberson, E.D., Höglinger, G.U., Koestler, M., Jack, C.R., Van Deerlin, V., Randolph, C., Lobach, I.V., Heuer, H.W., Gozes, I., Parker, L., Whitaker, S., Hirman, J., Stewart, A.J., Gold, M., Morimoto, B.H., AL-108-231 Investigators, 2014. Davunetide in patients with progressive supranuclear palsy: a randomised, double-blind, placebo-controlled phase 2/3 trial. Lancet Neurol. 13, 676–685. http://dx.doi.org/10.1016/S1474-4422(14)70088-2.

Bruns, M.B., Josephs, K.A., 2013. Neuropsychiatry of corticobasal degeneration and progressive supranuclear palsy. Int. Rev. Psychiatry 25, 197–209. http://dx.doi.org/10.3109/09540261.2013.766154. (Abingdon Engl.).

Burrell, J.R., Hodges, J.R., Rowe, J.B., 2014. Cognition in corticobasal syndrome and progressive supranuclear palsy: a review. Mov. Disord. 29, 684–693. http://dx.doi.org/10.1002/mds.25872.

Casanova, R., Srikanth, R., Baer, A., Laurienti, P.J., Burdette, J.H., Hayasaka, S., Flowers, L., Wood, F., Maldjian, J.A., 2007. Biological parametric mapping: a statistical toolbox for multimodality brain image analysis. NeuroImage 34, 137–143. http://dx.doi.org/10.1016/j.neuroimage.2006.09.011.

Chen, G., Saad, Z.S., Britton, J.C., Pine, D.S., Cox, R.W., 2013. Linear mixed-effects modeling approach to FMRI group analysis. NeuroImage 73, 176–190. http://dx.doi.org/10.1016/j.neuroimage.2013.01.047.

Choi, E.Y., Yeo, B.T.T., Buckner, R.L., 2012. The organization of the human striatum estimated by intrinsic functional connectivity. J. Neurophysiol. 108, 2242–2263. http://dx.doi.org/10.1152/jn.00270.2012.

Cole, D.M., Oei, N.Y.L., Soeter, R.P., Both, S., van Gerven, J.M., Rombouts, S.A.R.B., Beckmann, C.F., 2013. Dopamine-dependent architecture of cortico-subcortical network connectivity. Cereb. Cortex 23, 1509–1516. http://dx.doi.org/10.1093/cercor/bhs136.

Damoiseaux, J.S., Prater, K.E., Miller, B.L., Greicius, M.D., 2012. Functional connectivity tracks clinical deterioration in Alzheimer's disease. Neurobiol. Aging 33 (828). http://dx.doi.org/10.1016/j.neurobiolaging.2011.06.024. (e19–828.e30).

Dubois, B., Pillon, B., Legault, F., Agid, Y., Lhermitte, F., 1988. Slowing of cognitive processing in progressive supranuclear palsy. A comparison with Parkinson's disease. Arch. Neurol. 45, 1194–1199.

Dutt, S., Binney, R.J., Heuer, H.W., Luong, P., Attygalle, S., Bhatt, P., Marx, G.A., Elofson, J., Tartaglia, M.C., Litvan, I., McGinnis, S.M., Dickerson, B.C., Kornak, J., Waltzman, D., Voltarelli, L., Schuff, N., Rabinovici, G.D., Kramer, J.H., Jack, C.R., Miller, B.L., Rosen, H.J., Boxer, A.L., AL-108-231 investigators, 2016. Progression of brain atrophy in PSP and CBS over 6 months and 1 year. Neurology 87, 2016–2025. http://dx.doi.org/10.1212/WNL.0000000000003305.

Fogel, B.L., Clark, M.C., Geschwind, D.H., 2014. The neurogenetics of atypical parkinsonian disorders. Semin. Neurol. 34, 217–224. http://dx.doi.org/10.1055/s-0034-1381738.

Gardner, R.C., Boxer, A.L., Trujillo, A., Mirsky, J.B., Guo, C.C., Gennatas, E.D., Heuer, H.W., Fine, E., Zhou, J., Kramer, J.H., Miller, B.L., Seeley, W.W., 2013. Intrinsic connectivity network disruption in progressive supranuclear palsy. Ann. Neurol. 73, 603–616. http://dx.doi.org/10.1002/ana.23844.

Ghasemi, A., Zahediasl, S., 2012. Normality tests for statistical analysis: a guide for non-statisticians. Int. J. Endocrinol. Metab. 10, 486–489. http://dx.doi.org/10.5812/ijem.3505.

Ghosh, B.C.P., Calder, A.J., Peers, P.V., Lawrence, A.D., Acosta-Cabronero, J., Pereira, J.M., Hodges, J.R., Rowe, J.B., 2012. Social cognitive deficits and their neural correlates in progressive supranuclear palsy. Brain J. Neurol. 135, 2089–2102. http://dx.doi.org/10.1093/brain/aws128.

Golbe, L.I., 2014. Progressive supranuclear palsy. Semin. Neurol. 34, 151–159. http://dx.doi.org/10.1055/s-0034-1381736.

Golbe, L.I., Ohman-Strickland, P.A., 2007. A clinical rating scale for progressive supranuclear palsy. Brain 130, 1552–1565. http://dx.doi.org/10.1093/brain/awm032.

Greene, D.J., Laumann, T.O., Dubis, J.W., Ihnen, S.K., Neta, M., Power, J.D., Pruett, J.R., Black, K.J., Schlaggar, B.L., 2014. Developmental changes in the organization of functional connections between the basal ganglia and cerebral cortex. J. Neurosci. 34, 5842–5854. http://dx.doi.org/10.1523/JNEUROSCI.3069-13.2014.

Hedden, T., Gabrieli, J.D.E., 2010. Shared and selective neural correlates of inhibition, facilitation, and shifting processes during executive control. NeuroImage 51, 421–431. http://dx.doi.org/10.1016/j.neuroimage.2010.01.089.

Höglinger, G.U., Huppertz, H.-J., Wagenpfeil, S., Andrés, M.V., Belloch, V., León, T., del Ser, T., for the TAUROS MRI Investigators, 2014. Tideglusib reduces progression of brain atrophy in progressive supranuclear palsy in a randomized trial. Mov. Disord. 29, 479–487. http://dx.doi.org/10.1002/mds.25815.

Jack Jr., C.R., Knopman, D.S., Jagust, W.J., Petersen, R.C., Weiner, M.W., Aisen, P.S., Shaw, L.M., Vemuri, P., Wiste, H.J., Weigand, S.D., Lesnick, T.G., Pankratz, V.S., Donohue, M.C., Trojanowski, J.Q., 2013. Tracking pathophysiological processes in Alzheimer's disease: an updated hypothetical model of dynamic biomarkers. Lancet Neurol. 12, 207–216. http://dx.doi.org/10.1016/S1474-4422(12)70291-0.

Jahanshahi, M., Obeso, I., Rothwell, J.C., Obeso, J.A., 2015. A fronto-striato-subthalamic-pallidal network for goal-directed and habitual inhibition. Nat. Rev. Neurosci. http://dx.doi.org/10.1038/nrn4038.

Jones, D.T., Knopman, D.S., Gunter, J.L., Graff-Radford, J., Vemuri, P., Boeve, B.F., Petersen, R.C., Weiner, M.W., Jack, C.R., 2016. Cascading network failure across the Alzheimer's disease spectrum. Brain 139, 547–562. http://dx.doi.org/10.1093/brain/awv338.

Josephs, K.A., Xia, R., Mandrekar, J., Gunter, J.L., Senjem, M.L., Jack, C.R., Whitwell, J.L., 2013. Modeling trajectories of regional volume loss in progressive supranuclear palsy. Mov. Disord. 28, 1117–1124. http://dx.doi.org/10.1002/mds.25437.

Kertesz, A., McMonagle, P., 2010. Behavior and cognition in corticobasal degeneration and progressive supranuclear palsy. J. Neurol. Sci. In: Mental Dysfunction in Parkinson's Disease Proceedings of the 9th International Congress on Mental Dysfunction and other Non-Motor Features in Parkinson's Disease and Related Disorders. 289. pp. 138–143. http://dx.doi.org/10.1016/j.jns.2009.08.036.

Leisman, G., Moustafa, A.A., Shafir, T., 2016. Thinking, walking, talking: integratory motor and cognitive brain function. Front. Public Health 4, 94. http://dx.doi.org/10.3389/fpubh.2016.00094.

Levy, R., Dubois, B., 2006. Apathy and the functional anatomy of the prefrontal cortex–basal ganglia circuits. Cereb. Cortex 16, 916–928. http://dx.doi.org/10.1093/cercor/bhj043.

Levy, R., Goldman-Rakic, P.S., 2000. Segregation of working memory functions within the dorsolateral prefrontal cortex. In: Schneider, W.X., Owen, A.M., Duncan, J. (Eds.), Executive Control and the Frontal Lobe: Current Issues. Springer, Berlin Heidelberg, pp. 23–32.

Litvan, I., Agid, Y., Calne, D., Campbell, G., Dubois, B., Duvoisin, R.C., Goetz, C.G., Golbe, L.I., Grafman, J., Growdon, J.H., Hallett, M., Jankovic, J., Quinn, N.P., Tolosa, E., Zee, D.S., 1996. Clinical research criteria for the diagnosis of progressive supranuclear palsy (Steele-Richardson-Olszewski syndrome) Report of the NINDS-SPSP International Workshop*. Neurology 47, 1–9. http://dx.doi.org/10.1212/WNL.47.1.1.

Machulda, M.M., Jones, D.T., Vemuri, P., McDade, E., Avula, R., Przybelski, S., Boeve, B.F., Knopman, D.S., Petersen, R.C., Jack, C.R., 2011. Effect of APOE ε4 status on intrinsic network connectivity in cognitively normal elderly subjects. Arch. Neurol. 68, 1131–1136. http://dx.doi.org/10.1001/archneurol.2011.108.

McPherson, S., Fairbanks, L., Tiken, S., Cummings, J.L., Back-Madruga, C., 2002. Apathy and executive function in Alzheimer's disease. J. Int. Neuropsychol. Soc. 8, 373–381. http://dx.doi.org/10.1017/S1355617702813182.

Paviour, D.C., Price, S.L., Jahanshahi, M., Lees, A.J., Fox, N.C., 2006. Longitudinal MRI in progressive supranuclear palsy and multiple system atrophy: rates and regions of atrophy. Brain 129, 1040–1049. http://dx.doi.org/10.1093/brain/awl021.

Pillon, B., Blin, J., Vidailhet, M., Deweer, B., Sirigu, A., Dubois, B., Agid, Y., 1995. The neuropsychological pattern of corticobasal degeneration: comparison with progressive supranuclear palsy and Alzheimer's disease. Neurology 45, 1477–1483.

Power, J.D., Cohen, A.L., Nelson, S.M., Wig, G.S., Barnes, K.A., Church, J.A., Vogel, A.C., Laumann, T.O., Miezin, F.M., Schlaggar, B.L., Petersen, S.E., 2011. Functional network organization of the human brain. Neuron 72, 665–678. http://dx.doi.org/10.1016/j.neuron.2011.09.006.

Ridgway, G.R., Leung, K.K., Ashburner, J., 2015. Computing brain change over time. In: Toga, A.W. (Ed.), Brain Mapping. Academic Press, Waltham, pp. 417–428.

Rosen, H.J., Gorno-Tempini, M.L., Goldman, W.P., Perry, R.J., Schuff, N., Weiner, M., Feiwell, R., Kramer, J.H., Miller, B.L., 2002. Patterns of brain atrophy in frontotemporal dementia and semantic dementia. Neurology 58, 198–208.

Rubinov, M., Sporns, O., 2011. Weight-conserving characterization of complex functional brain networks. NeuroImage 56, 2068–2079. http://dx.doi.org/10.1016/j.neuroimage.2011.03.069.

Satterthwaite, T.D., Elliott, M.A., Gerraty, R.T., Ruparel, K., Loughead, J., Calkins, M.E., Eickhoff, S.B., Hakonarson, H., Gur, R.C., Gur, R.E., Wolf, D.H., 2013. An improved framework for confound regression and filtering for control of motion artifact in the preprocessing of resting-state functional connectivity data. NeuroImage 64, 240–256. http://dx.doi.org/10.1016/j.neuroimage.2012.08.052.

Seeley, W.W., Menon, V., Schatzberg, A.F., Keller, J., Glover, G.H., Kenna, H., Reiss, A.L., Greicius, M.D., 2007. Dissociable intrinsic connectivity networks for salience processing and executive control. J. Neurosci. 27, 2349–2356. http://dx.doi.org/10.1523/JNEUROSCI.5587-06.2007.

Segev-Jacubovski, O., Herman, T., Yogev-Seligmann, G., Mirelman, A., Giladi, N., Hausdorff, J.M., 2011. The interplay between gait, falls and cognition: can cognitive therapy reduce fall risk? Expert Rev. Neurotherapeutics 11, 1057–1075. http://dx.doi.org/10.1586/ern.11.69.

Shang, H., Shao, N., Yang, J., Li, J., 2014. Voxelwise meta-analysis of gray matter anomalies in progressive supranuclear palsy and Parkinson's disease using anatomic likelihood estimation. Front. Hum. Neurosci. 8, 63. http://dx.doi.org/10.3389/

fnhum.2014.00063.
Sheline, Y.I., Morris, J.C., Snyder, A.Z., Price, J.L., Yan, Z., D'Angelo, G., Liu, C., Dixit, S., Benzinger, T., Fagan, A., Goate, A., Mintun, M.A., 2010. APOE4 Allele disrupts resting state fMRI connectivity in the absence of amyloid plaques or decreased CSF A{beta}42. J. Neurosci. 30, 17035–17040. http://dx.doi.org/10.1523/JNEUROSCI.3987-10.2010.
Simioni, A.C., Dagher, A., Fellows, L.K., 2017. Effects of levodopa on corticostriatal circuits supporting working memory in Parkinson's disease. Cortex 93, 193–205. http://dx.doi.org/10.1016/j.cortex.2017.05.021.
Simmonds, D.J., Pekar, J.J., Mostofsky, S.H., 2008. Meta-analysis of Go/No-go tasks demonstrating that fMRI activation associated with response inhibition is task-dependent. Neuropsychologia 46, 224–232. http://dx.doi.org/10.1016/j.neuropsychologia.2007.07.015.
Steele, J.C., Richardson, J.C., Olszewski, J., 1964. Progression supranuclear palsy. A heterogenous degeneration involving the brain stem, basal ganglia adn cerebellum with vertical gaze and pseudobulbar palsy, nuchal dystonia and dementia. Arch. Neurol. 10, 333–359.
Vogt, B.A., Berger, G.R., Derbyshire, S.W.G., 2003. Structural and functional dichotomy of human midcingulate cortex. Eur. J. Neurosci. 18, 3134–3144.
Whitwell, J.L., Avula, R., Master, A., Vemuri, P., Senjem, M.L., Jones, D.T., Jack Jr., C.R., Josephs, K.A., 2011. Disrupted thalamocortical connectivity in PSP: a resting-state fMRI, DTI, and VBM study. Parkinsonism Relat. Disord. 17, 599–605. http://dx.doi.org/10.1016/j.parkreldis.2011.05.013.
Williams, D.R., de Silva, R., Paviour, D.C., Pittman, A., Watt, H.C., Kilford, L., Holton, J.L., Revesz, T., Lees, A.J., 2005. Characteristics of two distinct clinical phenotypes in pathologically proven progressive supranuclear palsy: Richardson's syndrome and PSP-parkinsonism. Brain 128, 1247–1258. http://dx.doi.org/10.1093/brain/awh488.
Williams, D.R., Holton, J.L., Strand, C., Pittman, A., de Silva, R., Lees, A.J., Revesz, T., 2007. Pathological tau burden and distribution distinguishes progressive supranuclear palsy-parkinsonism from Richardson's syndrome. Brain 130, 1566–1576. http://dx.doi.org/10.1093/brain/awm104.
Yeo, B.T.T., Krienen, F.M., Sepulcre, J., Sabuncu, M.R., Lashkari, D., Hollinshead, M., Roffman, J.L., Smoller, J.W., Zöllei, L., Polimeni, J.R., Fischl, B., Liu, H., Buckner, R.L., 2011. The organization of the human cerebral cortex estimated by intrinsic functional connectivity. J. Neurophysiol. 106, 1125–1165. http://dx.doi.org/10.1152/jn.00338.2011.